

A Facile One-Step Method for the Synthesis of Reduced Graphene Oxide Nanocomposites by NADH as Reducing Agent and Its Application in NADH Sensing

Mahmoud Amouzadeh Tabrizi,* Zahra Zand

Department of Chemistry, Institute for Advanced Studies in Basic Sciences, P.O. Box 45195-1159, Gava Zang, Zanjan, Iran
*e-mail: m.amouzadeh@iasbs.ac.ir

Received: July 29, 2013

Accepted: September 9, 2013

Published online: ■■ ■■, 2013

Abstract

Here, we report a green and eco-friendly approach to synthesize reduced graphene oxide (rGO) via a mild hydrothermal process using nicotinamide adenine dinucleotide (NADH) as a reducing agent. The obtained rGO was characterized by UV-visible absorption spectroscopy (UV-vis), X-ray diffraction spectroscopy, atomic force microscopy (AFM) and scanning electron microscopy (SEM). Electrochemical experiments indicated that the rGO/GC electrode exhibited an excellent electrocatalytic activity towards the oxidation of NADH, which can be attributed to the excellent electrical conductivity and high specific surface area of the rGO composite. The resulting biosensor showed highly sensitive amperometric response to NADH with a low detection limit (0.6 μM).

Keywords: Green chemistry, NADH, Reduced graphene oxide, Nanocomposites, Biosensors

DOI: 10.1002/elan.201300370

Supporting Information for this article is available on the WWW under <http://dx.doi.org/10.1002/elan.201300370>.

1 Introduction

Nicotinamide adenine dinucleotide (NADH) is a naturally occurring and vital compound found in all living cells of plants, animals, and humans. NADH is the body's top antioxidant, and can help with specific diseases such as Parkinson's [1], chronic fatigue syndrome [2], depression [3], and Alzheimer's disease [4]. Intracellular NAD^+ and NADH levels are also related to a number of brain [5] and sickle cell diseases [6]. Therefore, the determination of NADH is one of the important topics in biology, biochemistry and medicine. Several methods are available for the determination of NADH [7]. However, these methods are generally time-consuming, have a lack of sensitivity and a susceptibility to interference with other substances in analyte samples and are difficult for an automated detection. To overcome all these shortcomings, the electrochemical sensors based on carbon nanomaterials such as graphene and its derivatives are especially promising because of their simplicity, high sensitivity, selectivity and low over potential oxidation [8]. Graphene, a single aromatic sheet of sp^2 bonded carbon, has been shown to possess unique electronic, optical, thermal, mechanical and catalytic properties [9]. It has shown great application potential in various fields, such as ultracapacitors [10], batteries, [11] fuel cells [12] and bioscience/biotechnologies [13]. It is currently making an impact in the field of electrochemistry [14]. Most of the graphenes that

were chemically synthesized contain other elements, such as oxygen, so it is more reasonable to call this graphene "reduced graphene oxide" (rGO). This composite can be synthesized by various methods [15]. Among the current methods of generating rGO, hydrazine and sodium borohydride are used for the chemical reduction of exfoliated graphene oxide (GO) [16]. But, these reducing agents are unstable and dangerously toxic. Several research groups investigated the synthesis of rGO by eco-friendly methods, opening the door to application in nanoscience [15a–c,17]. Thus, the chemical reduction of exfoliated GO with green reducing agents has become a favorable topic for researchers. For example, reducing sugar [18], protein bovine serum albumin [19], heparin [20], poly(diallyldimethylammonium chloride) [21] dopamine derivatives [22] and 4-aminophenylboronic acid [23] perform well in reduction of GO. Therefore, an effective and green reducing agent for the chemical synthesis of soluble graphene is desirable. In this paper, we demonstrate a simple method to prepare rGO sheets in aqueous media by NADH as well as toxic agents. Also, the electrochemical behavior of NADH in phosphate buffer (PB) solution on rGO modified glassy carbon was studied. The prepared biosensor exhibited, fast response time, high stability, anti-fouling properties, lower detection limit and high sensitivity for NADH.

2 Experimental

2.1 Materials

All chemicals were of analytical reagent grade and used without further purification. High purity graphite powder (particle size <0.1 mm), H_3PO_4 , H_2SO_4 , KMnO_4 , HCl , KOH , KCl , $\text{K}_3[\text{Fe}(\text{CN})_6]$, $\text{K}_4[\text{Fe}(\text{CN})_6]$. Ethanol (96%) and ammonium hydroxide (25%) were obtained from Fluka (Buchs, Switzerland). NADH was obtained from Sigma. Double distilled water was used throughout.

2.2 Apparatus

Cyclic voltammetry and amperometric studies were performed using an Autolab potentiostat-galvanostat model PGSTAT30 (Eco Chemie, Utrecht, The Netherlands) with a conventional three electrode set-up, in which a rGO/GC electrode, an $\text{Ag}|\text{AgCl}|\text{KCl}_{\text{sat}}$ and a platinum rod served as the working, reference and auxiliary electrodes, respectively. The working potential was applied in the standard way using the potentiostat and the output signal was acquired by Autolab Nova software. Electrochemical impedance spectroscopy (EIS) experiments were carried out using a Zahner Zennium workstation in the presence of 5.0 mM $\text{Fe}(\text{CN})_6^{-3/-4}$ couple (1:1) as the redox probe. An oscillation potential of 5 mV over a frequency range of 100 kHz to 0.1 Hz was applied and the output signal was acquired with the Thales z (Zennium release) software. UV-visible (UV-vis) absorption spectra were recorded using a single beam Pharmacia UV-vis spectrophotometer (Ultraspec, model 4000). Scanning electron microscopy (SEM) was performed with a Philips instrument, Model XL-30 (Eindhoven, The Netherlands). Atomic force microscopy (AFM) measurements were made on DME DualScope Scanner DS 95-200 (Herlev, Denmark). X-ray diffraction (XRD) spectra were obtained using a D8ADVANCE (Bruker, Germany) using $\text{Cu K}\alpha$ (1.5406 Å) radiation. All measurements were performed at room temperature.

2.3 Preparation of the rGO Solution

Graphene oxide (GO) was synthesized using graphite powders by the modified Hummer's method [24]. Briefly, 5.0 g graphite powder was dispersed in a 120 mL concentrated H_2SO_4 and kept at 0°C under stirring. Then, 15.0 g of KMnO_4 was added gradually to the mixture kept in an ice bath to ensure that the temperature remained around 0°C. After that, the temperature was raised to 0°C and the mixture was stirred for 30 min and then diluted gradually with 225 mL deionized water. The mixture was rediluted with 700 mL deionized water and treated with 3% hydrogen peroxide. The color of the mixture changed to yellow-brown during the dropwise addition of H_2O_2 . The mixture was filtered and washed with HCl solution (5%) and then repeatedly washed with water until a neutral pH was obtained for the filtrate. This solution was centri-

fuged at 3000 rpm for 10 min and then the filtrate was re-dispersed in water and centrifuged for several times. Finally, a dark brown GO powder was obtained through drying at 50°C in a vacuum oven for a day. The graphite oxide was then exfoliated by ultrasonication. For this purpose, GO powder dispersed in a known volume of water was subjected to ultrasonication for 60 min to give a stable suspension of GO and then centrifuged at 3000 rpm for 30 min to remove any aggregates that remained in the transparent light brown exfoliated GO suspension.

Then, 0.5 mg of NADH was added into 3 mL exfoliated GO suspension (0.7 mg mL^{-1}) and the solution was mixed by ultrasonication for 30 min. The mixture was transferred into a vial, and the solution was stirred at 50°C for 2 h. During this process, the color of the solution changed from yellow-brown to black. The UV-vis spectra of GO solution containing NADH were recorded before and after process (Figure S1 Supporting Information). The absorbance peak, which is the characteristic band of NADH located at 335 nm, was gradually decreasing in during of reduction process and at the same time, absorbance peak at 257 nm was increased slightly, which is present of the formation of NAD^+ . The results provided the evidence of the oxidation process of NADH to NAD^+ . Adsorbed NADH and NAD^+ on rGO were extracted with ethanol and water by sonication and filtration condition, until no NADH/ NAD^+ could be detected in the washing solvent with an UV-vis spectrometer.

3 Results and Discussion

3.1 Characterization of the Composites

We monitored UV-vis absorption spectroscopy exfoliated GO (a) and rGO (b), firstly. As shown in Figure 1, the absorption peak at 230 nm showed red-shift to 271 nm after the exfoliated GO is reduced, indicating that the electronic conjugation within the rGO sheets was revived upon reduction of GO [18–21,24,25].

The effects of reduction time on the UV-vis absorption spectra of the GO dispersion (0.4 mg mL^{-1}) is shown also

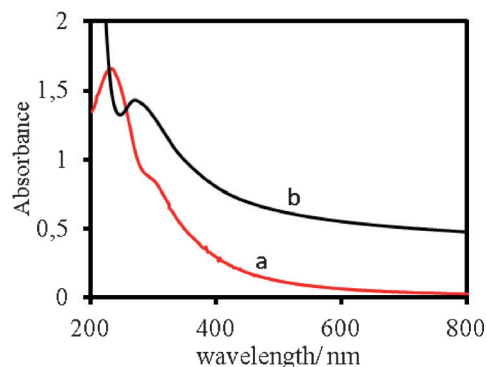


Fig. 1. UV-vis absorption spectra obtained from exfoliated GO solution (0.4 mg mL^{-1}) (a) and rGO solution (0.4 mg mL^{-1}) (b), respectively.

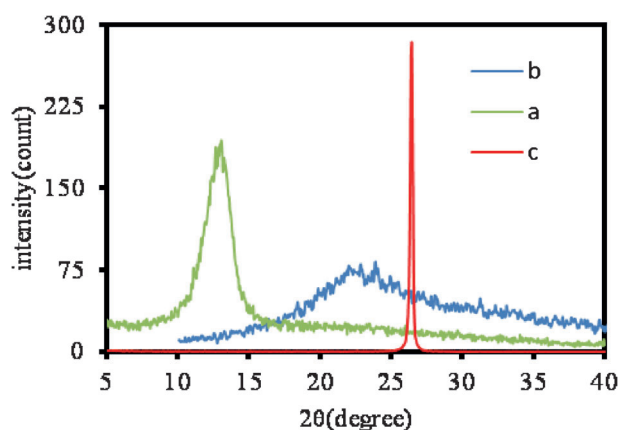


Fig. 2. Typical XRD patterns obtained from (a) exfoliated GO solution (0.4 mg mL^{-1}), (b) rGO solution (0.4 mg mL^{-1}) and (c) pristine graphite, respectively.

in Figure S2. With increasing reduction time, the absorption peak of GO was shifted from 230 nm for 0 min to 271 nm for 120 min, indicating the GO solution reduced to rGO solution in during of reduction reaction by NADH.

The obtained composites are also characterized by XRD. As shown in Figure 2, the XRD pattern of exfoliated GO (a) exhibits a diffraction peak centered at $2\theta = 13.01^\circ$, corresponding to the C(002) interlayer spacing of 0.78 nm, which indicates the complete oxidation of graphite to exfoliated GO [26]. After chemical reduction with NADH, the diffraction peak of exfoliated GO at $2\theta = 13.01^\circ$ disappeared and a very broad peak around 23° (b) was observed in the rGO sample, indicating that most oxygen functional groups had been removed [18,21,27]. It should be noted that the diffraction peak in rGO sheets were rather broad and significantly different from that in graphite(c) [26,28].

The morphological characterization of the prepared composites were examined by AFM and SEM. Figure 3 shows the typical AFM image of exfoliated GO (A) and rGO (B). The cross-sectional view indicates that the average thickness of exfoliated GO nanosheet is about 2.92 nm (Figure 3A). After the final reduction step, this value decreased to about 0.773 nm (Figure 3B), which could be attributed to the removal of the surface oxide groups. As previous report, the thickness of a single layer GO and rGO sheet are about 1 nm and 0.8 nm, respectively [29]. Therefore, unlike rGO, there are stacking effects in multilayer GO sheets.

The obtained SEM image of rGO is also shown in Figure 4. It can be seen that the basic shape of the rGO looks like a piece of a leave structure.

3.2 Preparation of rGO Modified GC Electrode

The end surface of a GC electrode (i.d. = 3.0 mm, Metrohm, Herisau, Switzerland) was polished on a synthetic cloth successively with 0.3, 0.1 and 0.05 μm alumina slurry

(Struers, Copenhagen, Denmark) to obtain a mirror finish and then cleaned in water-ethanol solution (1:1) under ultrasonication. A volume of 6 μL of the resulting rGO solution (0.4 mg mL^{-1}) was dropped onto a GC electrode and allowed to dry in ambient air for 2 h. The fabricated biosensor was stored at 4°C in a refrigerator when not in use.

3.3 Electrochemical Properties of the Electrodes

EIS and cyclic voltammetry (CV) have been used to characterize the interface properties of surface-modified electrodes. The typical impedance spectrum (presented in the form of the Nyquist plot) includes a semicircle portion at higher frequencies corresponding to the electron-transfer-limited process and a linear part at lower frequency range representing the diffusion limited process. The semicircle diameter in the impedance spectrum equals the electron-transfer resistance (R_{ct}). This resistance controls the electron-transfer kinetics of the redox probe at the electrode interface. Figure S3A (Supporting Information) displays the Nyquist plots obtained for a GC (a), rGO /GC (b) and GO/GC (c) electrodes in a solution containing 5.0 mM $\text{Fe}(\text{CN})_6^{-3/-4}$ couple (1:1) and 0.1 M KCl, respectively. The Nyquist diameter (R_{ct}) of rGO/GC electrode was much less than these observed for GC and GO/GC electrodes, suggesting that rGO facilitates the rate of electron transfer.

CV is also an efficient method for studying the interface properties of electrodes. CV studies showed (Figure 3 SB) that the observed peak to peak separation for the $\text{Fe}(\text{CN})_6^{-3/-4}$ redox couple on rGO/GC electrode (119 mV) was less than those observed for GO/GC electrode (197 mV) and GC electrode (207 mV). The peak current intensity on rGO/GC electrode was also higher than that observed on GO/GC electrode. The results were consistent with the EIS results. All these results demonstrated that rGO provide higher electron conduction pathways.

3.4 Electrochemical Oxidation of NADH at rGO/GC Electrode

Figure 5A shows CVs for the oxidation of NADH at these GC (a) and rGO/GC (b) electrodes. After modification of GC electrode with rGO, a remarkable increase in oxidation peak current was achieved. The peak potential of NADH oxidation is also shifted from 0.61 V at GC electrode to 0.35 V at rGO/GC electrode. Therefore, the peak potential of NADH at proposed electrode is slightly higher than 0.33 V at ionic liquid-functionalized graphene modified electrode [30]. This synergetic electrocatalytic activity toward NADH could be due to high conductivity, high surface area of rGO and, π - π stacking interaction between analyte with this nanocomposite. The OH and COH groups on rGO sheet can also form strong hydrogen-bonding interaction with OH and NH_2 groups in NADH. Figure 5B shows the CV responses of the rGO/

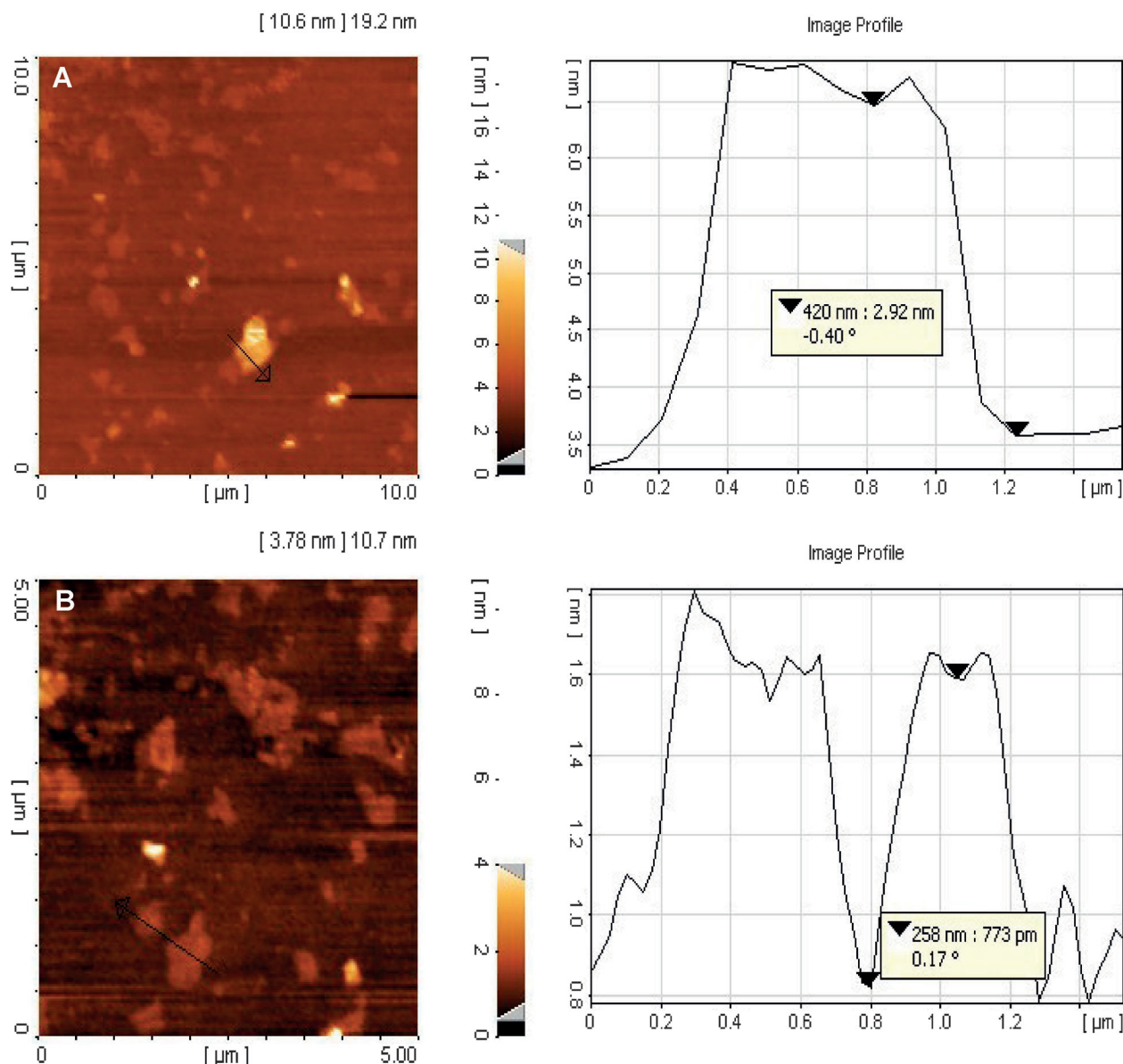


Fig. 3. Typical AFM image and surface profile obtained from GO solution (0.4 mg mL^{-1}) (A) and rGO (0.4 mg mL^{-1}) solution (B) deposited on a clean mica substrate.

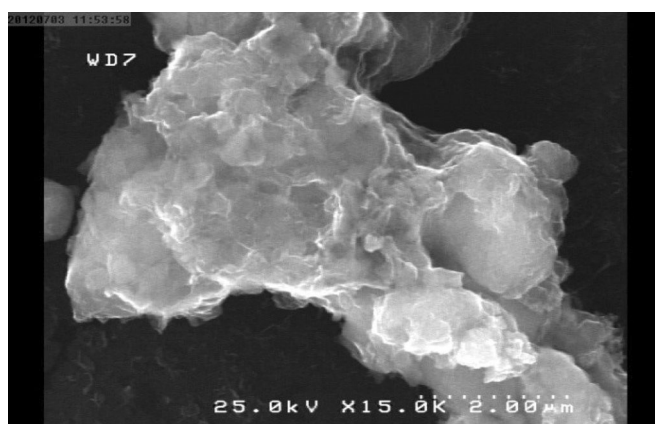


Fig. 4. SEM image obtained from rGO solution (0.4 mg mL^{-1}) deposited on a clean mica substrate.

GC electrode in PB solution containing NADH in various concentrations. It shows that the oxidation peak current increases as the NADH concentration increased. A linear relationship between the oxidation peak current and NADH concentration was obtained for the concentration range of 0 to $400 \mu\text{M}$ with a correlation coefficient of 0.9992 (Figure 5B Inset).

Figure 5C displays the influence of scan rate on the current response of the anodic current of $200 \mu\text{M}$ NADH. The anodic peak current (i_{pa}) increased upon the increase of the square root of scan rate ($v^{1/2}$). The result indicates that the electrochemical kinetics is controlled by the diffusion of NADH.

The Tafel slope can be obtained by following equation that is valid for a totally irreversible diffusion controlled process [31]: $E_p = b/2 \log(v) + \text{constant}$ where b indicates

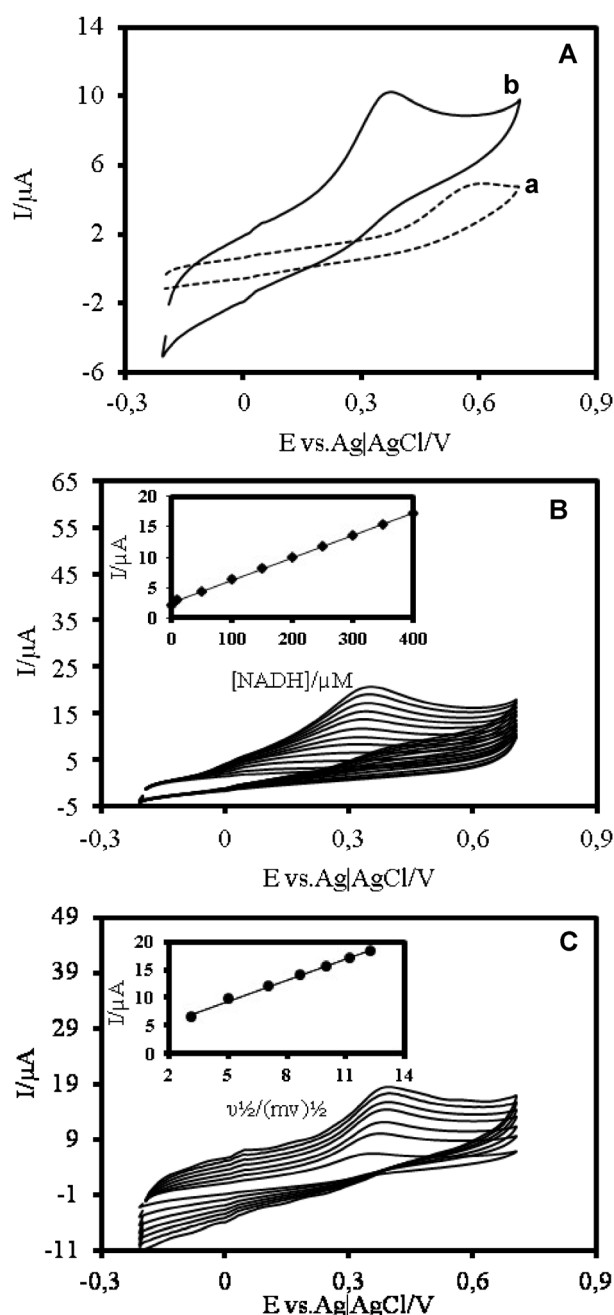


Fig. 5. (A) Cyclic voltammograms of GC electrode (a) and rGO/GC electrode (b) in a solution containing 200 μM NADH at a scan rate of 25 mV s^{-1} . (B) Cyclic voltammograms of a rGO/GC electrode in PB solution (0.1 M and pH 7.0) containing different amounts of NADH from 0 to 400 μM at a scan rate of 25 mV s^{-1} . (C) Cyclic voltammograms of 200 μM NADH at various scan rates. Inset (Figure 5C): Linear dependence of anodic peak currents versus square root of scan rate ($v^{1/2}$) in the range from 10 to 150 mV s^{-1} . The data were recorded in PB solution (0.1 M, pH 7.0).

the Tafel slope. According to this equation, the evaluated slope of E_p vs. $\log v$ is $-0.0867 \text{ V decade}^{-1}$; therefore, $b = 0.1734 \text{ V decade}^{-1}$. So the amount of transfer coefficient (α) was estimated as 0.34 (Figure S4, Supporting Information).

3.5 Amperometric Detection of NADH

Chronoamperometry can be used for the evaluation of the catalytic reaction rate constant (k_{cat}) using the following equation $I_{\text{cat}}/I_L = \pi^{1/2}(k_{\text{cat}}c_0t)^{1/2}$. Where, I_{cat} is the catalytic current of the rGO/GC electrode in the presence of NADH, I_L is the limiting current in the absence of NADH, and k_{cat} , c_0 , and t are the catalytic rate constant ($\text{M}^{-1}\text{s}^{-1}$), catalyst concentration (M) and time elapsed (s), respectively. From the slope of the I_{cat}/I_L vs. $t^{1/2}$ plot we can simply calculate the value of k_{cat} for a given concentration of substrate. The average value of k_{cat} for a chemical reaction of NADH at rGO/GC electrode was found to be $0.172 \times 10^5 \text{ cm}^{-3}\text{s}^{-1}$ (Figure S5, Supporting Information).

For an electroactive material with a diffusion coefficient (D), the current response under diffusion controlled condition is described by the Cottrell equation [27] $I = nFAC(D/\pi t)^{1/2}$, where n is the number of electrons; F is the Faraday constant; A is the electrode area; C is the bulk concentration of analyte; D is the diffusion coefficient of analyte in solution; t is the time. The slope of the initial part of the I vs. $t^{-1/2}$ plot can be used for the estimation of the diffusion coefficient (D) of NADH. The mean value of D was found to be $2.24 \times 10^{-7} \text{ cm}^2\text{s}^{-1}$. The estimated diffusion coefficient is smaller than theoretical value, indicating the efficient electrooxidation of NADH on the surface of electrode.

The amperometric responses of the rGO/GC and GC electrodes were investigated by successive addition of NADH to a continuously stirred 0.1 M PB solution at the applied potential of +0.35 V versus Ag|AgCl|KCl_{sat} (Figure 6A). It can be seen that the current responses of the GC electrode (curve a) was very small compared to that of the rGO/GC electrode (curve b). The current responses of the rGO/GC biosensor increased with increasing NADH concentration (Figure 6B). The calibration curve of this biosensor gave a linear range of the concentration of NADH from 0 to 500 μM . The linear regression equation was $i (\mu\text{A}) = 0.0256 [\text{NADH}] (\mu\text{M}) + 1.28$ with a correlation coefficient of 0.998 ($n = 11$). The limit of detection was estimated at a signal-to-noise ratio of 3 to be 0.6 μM . The sensor responds rapidly to the substrate, as about 95% of the steady-state current is obtained within 2 s. This detection limit is much lower than most of previously reported values for NADH sensors based on graphene [8a,b,32]. The significantly improved performance of the sensor may be attributed to the presence of a large amount of edges on rGO, causing a rough and porous surface of the rGO/GC electrode.

The sensor characteristics compared with other graphene modified electrodes used in the electrocatalysis of NADH are summarized in Table 1.

The selective detection of NADH is also very important in the fabrication of a NADH sensor. Therefore, the effect of the co-existing electroactive ascorbic acid (AA) on the detection of NADH was investigated by CV. As shown in Figure S6 (Supporting Information), two well

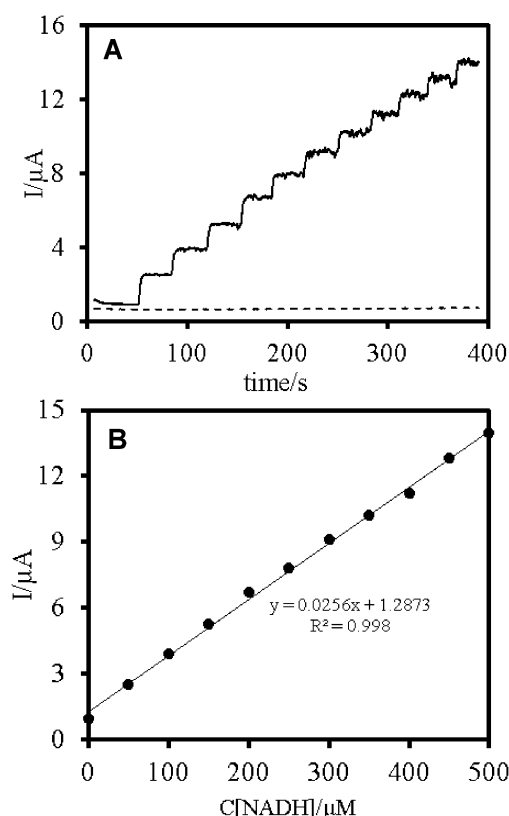


Fig. 6. (A) Amperometric responses of GC electrode (a) and rGO/GC electrode (b) in 0.1 M PB solution (pH 7.0) to successive additions of NADH. (B) Calibration curve of rGO/GC electrode. Applied potential: +0.35 V versus Ag|AgCl|KCl_{sat}.

defined peaks are observed for AA (100 μM) and NADH (100 μM). So, rGO/GC electrode can be used for determination of NADH without interference from AA. The rGO/GC electrode exhibited also good reproducibility in the detection of NADH with a relative standard deviation (RSD) of ca. 1.83% found over 6 repeated measurements of 100 μM NADH. Anti-fouling property is one of the most important properties for sensor application. Figure S7 (Supporting Information) compares the amperometric responses of the bare GC and rGO/GC electrodes to 100 μM NADH at +0.35 V recorded over a continuous period of 400 s. This figure shows that the response of the rGO/GC electrode remains stable after 400 s. In contrast, the response of GC electrode decays (nearly 35% after 400 s), indicating a serious inhibition of the oxidation pro-

cess. When not in use, the rGO/GC electrode was stored at room temperature in PB solution. No obvious change for CV response was observed after 14 days. The electrochemical sensor was also used for the determination of NADH in urine sample. Briefly, 2.0 mL of the filtered urine solution added to 8.0 mL of PB solution (0.1 M, pH 7.0). Then, the solution was transferred into the voltammetric cell to be analyzed. After that, 10 μL of NADH (0.1 M) injected to this cell and amperometric analysis has done by proposed sensor. The recovery of the analysis was about 102%, considering the value determined by standard method [34].

4 Conclusions

In this study, we proposed the one-step synthesis of rGO by using NADH as a reducing agent. UV-vis, and XRD spectra indicate the conversion of GO to rGO via an eco-friendly chemical reduction method. The rGO modified electrode exhibited a higher electrocatalytic activity towards NADH. The kinetics of the catalytic reaction has been explained using cyclic voltammetry and chronoamperometry. The rGO/GC electrode exhibited a linear response to NADH within the concentration range of 0–500 μM and a low detection limit (0.6 μM). The proposed electrode displayed also a good stability, selectivity and anti-fouling properties.

Acknowledgements

The author thank Dr P. Marashi and Miss Somayeh Jalilzadeh from Maharfan Abzar Co (Tehran, Iran) for the support with the AFM system. We would like to thank Dr Behzad Haghighi for all his advice.

References

- [1] W. Birkmayer, G. J. Birkmayer, *Ann. Clin. Lab. Sci.* **1989**, 19, 38.
- [2] L. M. Forsyth, H. G. Preuss, A. L. MacDowell, L. Chiazzie, G. D. Birkmayer, J. A. Bellanti, *Ann. Allergy, Asthma Immunol.: Off. Publ. Am. Coll. Allergy, Asthma, Immunol.* **1999**, 82, 185.
- [3] A. Rex, L. Pfeifer, F. Fink, H. Fink, *J. Neurosci. Res.* **1999**, 57, 359.
- [4] C. Pocernich, D. A. Butterfield, *Neurotox. Res.* **2003**, 5, 515.

Table 1. Comparison of the performance of the rGO/GC electrode for the electrochemical detection of NADH with that of other rGO modified electrodes.

Working electrode	Applied potential (V) vs. Ag/AgCl	Linear range (μM)	Detection limit (μM)	References
Chemically reduced graphene oxide/GC electrode	+0.45	40–800	10	[32b]
Peptide nanowires–graphene/GC electrode	+0.5	50–600	1.2	[33]
Ionic liquid functionalized graphene/GC electrode	+0.45	250–2000	–	[8a]
Au–RGO/Chit modified GC electrode	+0.35	1.5–320	1.2	[8b]
rGO/GC electrode	+0.35	0–500	0.6	This work

- [5] P. Belenky, K. L. Bogan, C. Brenner, *Tr. Biochem. Sci.* **2007**, 32, 12.
- [6] C. R. Zerez, N. A. Lachant, K. R. Tanaka, *Blood* **1990**, 76, 1008.
- [7] a) Y. Li, X. Yang, F. Yang, Y. Wang, P. Zheng, X. Liu, *Electrochim. Acta* **2012**, 66, 188; b) L. Tang, X. Lei, G. Zeng, Y. Liu, Y. Peng, M. Wu, Y. Zhang, C. Liu, Z. Li, G. Shen, *Spectrochim. Acta A, Mol. Biomol. Spectrosc.* **2012**, 99, 390; c) D. G. Dilgin, D. Gligor, H. İ. Gökçel, Z. Dursun, Y. Dilgin, *Biosens. Bioelectron.* **2010**, 26, 411; d) C. Brugidou, A. Rocher, E. Giraud, B. Lelong, B. Marin, M. Raimbault, *Biotechnol. Tech.* **1991**, 5, 475.
- [8] a) C. Shan, H. Yang, D. Han, Q. Zhang, A. Ivaska, L. Niu, *Biosens. Bioelectron.* **2010**, 25, 1504; b) H. Chang, X. Wu, C. Wu, Y. Chen, H. Jiang, X. Wang, *Analyst* **2011**, 136, 2735; c) K. Guo, K. Qian, S. Zhang, J. Kong, C. Yu, B. Liu, *Talanta* **2011**, 85, 1174.
- [9] a) A. K. Geim, K. S. Novoselov, *Nat. Mater.* **2007**, 6, 183; b) A. K. Geim, *Science* **2009**, 324, 1530.
- [10] a) M. D. Stoller, S. Park, Y. Zhu, J. An, R. S. Ruoff, *Nano Lett.* **2008**, 8, 3498; b) D.-W. Wang, F. Li, J. Zhao, W. Ren, Z.-G. Chen, J. Tan, Z.-S. Wu, I. Gentle, G. Q. Lu, H.-M. Cheng, *ACS Nano* **2009**, 3, 1745; c) Y. Wang, Z. Shi, Y. Huang, Y. Ma, C. Wang, M. Chen, Y. Chen, *J. Phys. Chem. C* **2009**, 113, 13103.
- [11] E. Yoo, J. Kim, E. Hosono, H.-s. Zhou, T. Kudo, I. Honma, *Nano Lett.* **2008**, 8, 2277.
- [12] a) B. Seger, P. V. Kamat, *J. Phys. Chem. C* **2009**, 113, 7990; b) R. Kou, Y. Shao, D. Wang, M. H. Engelhard, J. H. Kwak, J. Wang, V. V. Viswanathan, C. Wang, Y. Lin, Y. Wang, I. A. Aksay, J. Liu, *Electrochem. Commun.* **2009**, 11, 954; c) E. Yoo, T. Okata, T. Akita, M. Kohyama, J. Nakamura, I. Honma, *Nano Lett.* **2009**, 9, 2255; d) Y. Si, E. T. Samulski, *Chem. Mater.* **2008**, 20, 6792; e) Y. Li, L. Tang, J. Li, *Electrochem. Commun.* **2009**, 11, 846.
- [13] a) Z. Liu, J. T. Robinson, X. Sun, H. Dai, *J. Am. Chem. Soc.* **2008**, 130, 10876; b) H. Chen, M. B. Müller, K. J. Gilmore, G. G. Wallace, D. Li, *Adv. Mater.* **2008**, 20, 3557; c) C. Shan, H. Yang, J. Song, D. Han, A. Ivaska, L. Niu, *Anal. Chem.* **2009**, 81, 2378; d) Z. Wang, X. Zhou, J. Zhang, F. Boey, H. Zhang, *J. Phys. Chem. C* **2009**, 113, 14071; e) L. Tang, Y. Wang, Y. Li, H. Feng, J. Lu, J. Li, *Adv. Funct. Mater.* **2009**, 19, 2782; f) X. Kang, J. Wang, H. Wu, I. A. Aksay, J. Liu, Y. Lin, *Biosens. Bioelectron.* **2009**, 25, 901.
- [14] a) X. Chen, J. Zhu, Q. Xi, W. Yang, *Sens. Actuators B, Chem.* **2012**, 161, 648; b) H. Fan, Y. Li, D. Wu, H. Ma, K. Mao, D. Fan, B. Du, H. Li, Q. Wei, *Anal. Chim. Acta* **2012**, 711, 248; c) J. Li, D. Kuang, Y. Feng, F. Zhang, Z. Xu, M. Liu, *J. Hazardous Mater.* **2012**, 201–202, 250; d) C. Wu, D. Sun, Q. Li, K. Wu, *Sens. Actuators B, Chem.* **2012**, 168, 178; e) G.-H. Wu, Y.-F. Wu, X.-W. Liu, M.-C. Rong, X.-M. Chen, X. Chen, *Anal. Chim. Acta* **2012**, 745, 337; f) Y. Hu, X. Li, D. Geng, M. Cai, R. Li, X. Sun, *Electrochim. Acta* **2013**, 91, 227; g) Y. Jiang, D. Chen, J. Song, Z. Jiao, Q. Ma, H. Zhang, L. Cheng, B. Zhao, Y. Chu, *Electrochim. Acta* **2013**, 91, 173; h) M. Pumera, A. Ambrosi, A. Bonanni, E. L. K. Chng, H. L. Poh, *TrAC – Tr. Anal. Chem.* **2010**, 29, 954.
- [15] a) K. S. Kim, Y. Zhao, H. Jang, S. Y. Lee, J. M. Kim, K. S. Kim, J.-H. Ahn, P. Kim, J.-Y. Choi, B. H. Hong, *Nature* **2009**, 457, 706; b) C. E. Hamilton, J. R. Lomeda, Z. Sun, J. M. Tour, A. R. Barron, *Nano Lett.* **2009**, 9, 3460; c) M. Lotya, P. J. King, U. Khan, S. De, J. N. Coleman, *ACS Nano* **2010**, 4, 3155; d) M. Choucair, P. Thordarson, J. A. Stride, *Nat. Nano* **2009**, 4, 30; e) S. Stankovich, D. A. Dikin, G. H. B. Dommett, K. M. Kohlhaas, E. J. Zimney, E. A. Stach, R. D. Piner, S. T. Nguyen, R. S. Ruoff, *Nature* **2006**, 442, 282.
- [16] a) S. Stankovich, D. A. Dikin, R. D. Piner, K. A. Kohlhaas, A. Kleinhammes, Y. Jia, Y. Wu, S. T. Nguyen, R. S. Ruoff, *Carbon* **2007**, 45, 1558; b) X. Gao, J. Jang, S. Nagase, *J. Phys. Chem. C* **2009**, 114, 832.
- [17] a) Y. Huang, J. Liang, Y. Chen, *J. Mater. Chem.* **2012**, 22, 3671; b) W. Zhang, F. Tan, W. Wang, X. Qiu, X. Qiao, J. Chen, *J. Hazardous Mater.* **2012**, 217–218, 36.
- [18] X. Xie, K. Zhao, X. Xu, W. Zhao, S. Liu, Z. Zhu, M. Li, Z. Shi, Y. Shao, *J. Phys. Chem. C* **2010**, 114, 14243.
- [19] J. Liu, S. Fu, B. Yuan, Y. Li, Z. Deng, *J. Am. Chem. Soc.* **2010**, 132, 7279.
- [20] Y. Wang, P. Zhang, C. Fang Liu, L. Zhan, Y. Fang Li, C. Z. Huang, *RSC Advances* **2012**, 2, 2322.
- [21] S. Zhang, Y. Shao, H. Liao, M. H. Engelhard, G. Yin, Y. Lin, *ACS Nano* **2011**, 5, 1785.
- [22] a) I. Kaminska, M. R. Das, Y. Coffinier, J. Niedziolka-Jonsson, J. Sobczak, P. Woisel, J. Lyskawa, M. Opallo, R. Boukherroub, S. Szunerits, *ACS Appl. Mater. Interf.* **2012**, 4, 1016; b) I. Kaminska, W. Qi, A. Barras, J. Sobczak, J. Niedziolka-Jonsson, P. Woisel, J. Lyskawa, W. Laure, M. Opallo, M. Li, R. Boukherroub, S. Szunerits, *Chem. Eur. J.* **2013**, 19, 8673.
- [23] Q. Wang, I. Kaminska, J. Niedziolka-Jonsson, M. Opallo, M. Li, R. Boukherroub, S. Szunerits, *Biosens. Bioelectron.* **2013**, 50, 331.
- [24] W. S. Hummers, R. E. Offeman, *J. Am. Chem. Soc.* **1958**, 80, 1339.
- [25] a) M. L. Andersen, H. Outtrup, L. H. Skibsted, *J. Agric. Food Chem.* **2000**, 48, 3106; b) J. A. Vinson, M. Mandarano, M. Hirst, J. R. Trevithick, P. Bose, *J. Agric. Food Chem.* **2003**, 51, 5528; c) Y. Zhou, Q. Bao, L. A. L. Tang, Y. Zhong, K. P. Loh, *Chem. Mater.* **2009**, 21, 2950.
- [26] H.-L. Guo, X.-F. Wang, Q.-Y. Qian, F.-B. Wang, X.-H. Xia, *ACS Nano* **2009**, 3, 2653.
- [27] a) H. M. A. Hassan, V. Abdelsayed, A. E. R. S. Khder, K. M. AbouZeid, J. Terner, M. S. El-Shall, S. I. Al-Resayes, A. A. El-Azhary, *J. Mater. Chem.* **2009**, 19, 3832; b) M. J. McAllister, J.-L. Li, D. H. Adamson, H. C. Schniepp, A. A. Abdala, J. Liu, M. Herrera-Alonso, D. L. Milius, R. Car, R. K. Prud'homme, I. A. Aksay, *Chem. Mater.* **2007**, 19, 4396.
- [28] H. Yang, C. Shan, F. Li, D. Han, Q. Zhang, L. Niu, *Chem. Commun.* **2009**, 0, 3880.
- [29] P. Cui, S. Seo, J. Lee, L. Wang, E. Lee, M. Min, H. Lee, *ACS Nano* **2011**, 5, 6826.
- [30] C. Shan, H. Yang, D. Han, Q. Zhang, A. Ivaska, L. Niu, *Biosens. Bioelectron.* **2010**, 25, 1504.
- [31] L. R. F. A. J. Bard, *Electrochemical Methods, Fundamentals and Applications*, Wiley, New York **1980**.
- [32] a) W.-J. Lin, C.-S. Liao, J.-H. Jhang, Y.-C. Tsai, *Electrochem. Commun.* **2009**, 11, 2153; b) M. Zhou, Y. Zhai, S. Dong, *Anal. Chem.* **2009**, 81, 5603; c) G. P. Keeley, A. O'Neill, M. Holzinger, S. Cosnier, J. N. Coleman, G. S. Duesberg, *Phys. Chem. Chem. Phys.* **2011**, 13, 7747.
- [33] P. Li, X. Chen, W. Yang, *Langmuir* **2013**, 29, 8629.
- [34] T. Ohno, M. Suzuki, T. Horiuchi, Y. Shirahase, K. Kishi, Y. Watazu, *U.S. Patent US005250416A*, Oct. 5, **1993**.